Journal of Applied Electrochemistry (2021) 51:1689–1703
https://doi.org/10.1007/s10800-021-01607-4

RESEARCH ARTICLE

# Electrocatalytic cleavage of a carbon–chlorine bond by Re(IV)–chloro complex: a mechanistic insight from DFT

**Jamaladin Shakeri[1] · Hassan Hadadzadeh[1] · Hossein Farrokhpour[1] · Matthias Weil[2] · Mohammad Joshaghani[3]**

Received: 1 January 2021 / Accepted: 18 July 2021 / Published online: 27 July 2021


## Abstract

A new mononuclear hexachlororhenate complex salt ((2-ppyH)$_2$[ReCl$_6$], where 2-ppyH$^+$ = 2-phenylpyridinium cation) was synthesized and structurally characterized by X-ray crystallography. The hexachlororhenate complex ([ReCl$_6$]$^{2-}$) was utilized as an efficient catalyst for the electrocatalytic dechlorination of dichloromethane ($CH_2Cl_2$). The cyclic voltammograms (CVs) in the presence of CH2Cl2 show catalytic cathodic currents in place of the reversible wave for the redox pair Re(IV)/Re(III). The controlled potential electrolysis was also employed to study the catalytic carbon–chloride (C–Cl) bond cleavage of $CH_2Cl_2$ in the presence of [ReCl$_6$]$^{2-}$. The major electrolysis product was characterized as 1,2-dichloroethane (EDC), determined by gas chromatography–mass spectrometry (GC–MS). According to the cyclic voltammetry data, an electrocatalytic mechanism was proposed using the density functional theory (DFT, M06-L) to investigate the cleavage of the C–Cl bond in the presence of hexachlororhenate(IV). The optimized structures and the $\Delta G^\circ$ changes ($\Delta G^\circ_g$ and $\Delta G^\circ_{sol}$) for the proposed mechanism were calculated. Accordingly, the electrochemical pathway was thermodynamically feasible in both gas and solvent (acetonitrile) phases. The DFT studies suggest that the chlorine elimination proceeds through an interaction between the chlorine atom of $CH_2Cl_2$ and the five-coordinated unsaturated rhenium (III) intermediate. The transition state for the transfer of chlorine to the Re center was located with the assessed barrier energy of + 16.53 kJ mol$^{-1}$ in the solvent phase.

✉ Hassan Hadadzadeh
hadad@iut.ac.ir

[1] Department of Chemistry, Isfahan University of Technology, 84156-83111 Isfahan, Iran

[2] Institute of Chemical Technologies and Analytics, Division of Structural Chemistry, TU Wien, Getreidemarkt 9/164-SC, 1060 Vienna, Austria

[3] Faculty of Chemistry, Razi University, 67149 Kermanshah, Iran

**Graphic abstract**

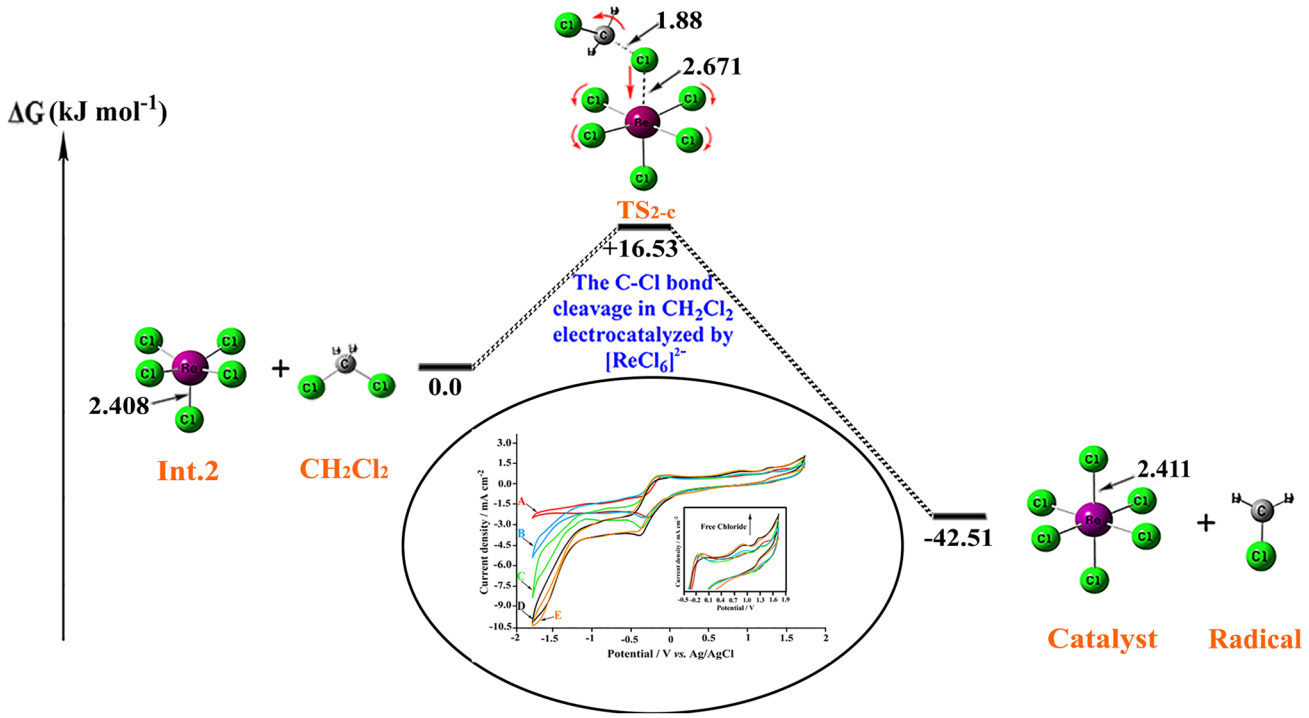


**Keywords** C–Cl bond cleavage · Electrocatalytic reaction · Density functional theory · Mechanistic insight

## 1 Introduction

Chlorinated organic compounds are widely employed in chemical and industrial applications such as solvents, pesticides, adhesives, pharmaceuticals, and polymers [1–3]. Many of these compounds have been identified as persistent organic pollutants (POPs) [4–7]. These organics contain various types of carbon-chlorine bonds such as aliphatics (chlordane), aromatics (hexachlorobenzene), polychlorinated compounds (polychlorinated biphenyls), and chlorinated volatile organic halides (chloroform and dichloromethane). They have gained increasing concerns due to their toxic nature, bioaccumulation, and durability, resulting in threats to aquatic environments and human health [8–11]. Some of the most chlorinated compounds were banned by the Stockholm convention [12], because of their potential harmful carcinogenic and mutagenic effects [13]. Due to their recalcitrant properties and poor biodegradability, they can remain persistent in soil and water for several years [14]. Hence, efficient techniques for the removal or conversion of these organic pollutants are in demand. In particular, reduction of organic halides by the electrochemical method is one of the most promising techniques for the treatment of POPs and pollution remedy [15, 16]. In the last decade, there has been increased attention in applying electrocatalytic degradation methods for possible conversion or removal of environmental pollutants. Electrochemical processes have been considered highly effective for the dechlorination of organic chlorinated pollutants [2, 17]. The electrocatalytic reduction of chlorofluorocarbons (CFCs) has been widely investigated by numerous researchers [18–20]. For instance, the catalytic electroreduction of trichlorotrifluoroethane (CFC-113) in different solvents, including $CH_3CN$, propylene carbonate, DMF, and DMF/$H_2O$, was studied by Peters and co-workers [19]. Sun et al. [21] investigated the effective electrocatalytic dechlorination processes of chlorophenols compounds at a Pd–Ni bimetallic cathode. A titanium nitride doped palladium/nickel foam electrode was examined for the dechlorination of 2,4-dichlorophenoxyacetic acid, in which the electrode was able to dechlorinate 71% of the initially added 2,4-dichlorophenoxyacetic acid within one hour. In recent years, research has been carried out on the electrochemical reductive dechlorination of organic halides in solution. Several scientists have developed electrochemical dechlorination reactions utilizing homogeneous catalysts in form of metal complexes [22–26]. Peters et al. [27] investigated electrocatalytic reduction of 1,1,1-trichloro-2,2-bis(4-methoxyphenyl)

ethane (methoxychlor pesticide) by $Ni^{I}$(salen) complex (salen = N,N′-ethylenebis(salicylimine)) at a glassy carbon (GC) cathode, in which 32% of the products were completely dechlorinated. In another study, Peters′s group [28] studied the $Ni^{I}$(salen)-catalyzed reduction of CFC-113 to CFC-1113 (1-chloro-1,2,2-trifluoroethene) in dimethylformamide with a high reaction yield of 99%. Similar to $Ni^{I}$(salen), $Co^{I}$(salen) complexes are other widely investigated catalysts in the cleavage of carbon–chlorine bonds [29]. Gach et al. [30] studied the electrocatalytic conversion of hexachlorobenzene and pentachlorobenzene to corresponding products by $Co^{I}$(salen) at a GC cathode. Also, the anionic complex hexachloropalladate(IV) ($[PdCl_6]^{2-}$) plays a catalytic role in the electrolytic dechlorination of 2-chlorobiphenyl at a graphite electrode [31]. Brown et al. [32] performed the conversion of chlorinated solvents to radical species in the presence of hexachlororhenate(IV) as the catalyst via an electrocatalytic reduction reaction, which can be considered as an electrocatalytic method for generating radicals from organic chlorides [32]. Besides, there are many reports on the mechanism of the reductive cleavage of the C–X bonds (X = halogen) through electrochemical reactions [33–35]. The reductive cleavage of the C–X bond may proceed via two potential pathways: a stepwise pathway, which belongs to a major part of aryl halides and involves the intermediate formation of a radical anion ($RX^{\cdot -}$) or the single-step concerted process, which is limited to the alkyl halides [36].

$$R{-}X + e^- \rightleftharpoons [RX^{\cdot -}] \rightarrow R^{\cdot} + X^- \quad \text{(stepwise)} \quad (1)$$

$$R - X + e^- \rightarrow R^{\cdot} + X^- \quad \text{(concerted)} \quad (2)$$

The mechanism of the copper-catalyzed reductive cleavage of the carbon-halogen bond was investigated by Coote et al. [33], in which electron transfer and bond breaking of the alkyl halide occurred in a single step. Gennaro and coworkers [37] performed a computational evaluation of the electrochemical properties of alkyl halides in the presence of a $Cu^{I}$/TPMA complex. It should be mentioned that the electron transfer occurs by an inner-sphere electron transfer (ISET) pathway in both mechanisms. However, it was shown that the electrocatalytic dechlorination mechanism of chlorinated solvents catalyzed by Re(IV)-chloride does not proceed through an intermolecular electron transfer [32]. This mechanism includes the abstraction of a chlorine atom from the substrate by a highly reactive coordinatively unsaturated $Re^{III}$ intermediate [32].

In this work, the synthesis of a new mononuclear hexachlororhenate complex salt, ($(2\text{-ppyH})_2[ReCl_6]$), and its electrocatalytic activity on the dechlorination of $CH_2Cl_2$ are reported. The bulk electrolysis has been utilized to investigate the catalytic remediation of $CH_2Cl_2$ by the $Re^{IV}$ catalyst, which is electrogenerated at a platinum electrode in acetonitrile containing 0.1 M tetrabutylammonium hexafluorophosphate. In addition, theoretical details of the electrocatalytic mechanism for the dechlorination of $CH_2Cl_2$ in the presence of $[ReCl_6]^{2-}$ as the catalyst are presented. In comparison with previous research [25, 31, 32], the present study contains the following advancements, a proposal of an electrocatalytic mechanism for the cleavage of the C–Cl bond of $CH_2Cl_2$ in the presence of hexachlororhenate(IV), the determination of the transition state structures, the calculation of turnover number (TON) for the electrocatalytic dechlorination of $CH_2Cl_2$, the synthesis and complete characterization of a new Re(IV) complex, and the evaluation of the effect of reaction parameters on the electrocatalytic reaction yield.

## 2 Experimental

### 2.1 Materials and measurements

2–Phenylpyridine (ppy), silver nitrate, $ReCl_5$ ($Re_2Cl_{10}$), tetrabutylammonium hexafluorophosphate (TBAH), ferrocene (Fc), acetonitrile (MeCN), chloroform, DMF, and hexane were purchased from Sigma Aldrich. FT-IR and $^1H$ NMR spectra and elemental analysis were carried out on FT-IR JASCO 680-PLUS and Bruker Avance III-400 NMR spectrometers, and a Leco, CHNS-932 instrument, respectively. GC and GC–MS analyses were recorded on an Agilent 6890 N GC (equipped with FID and an HB-$50^+$ column) and an Agilent 7890A/5975C GC–MS instrument with an HP-5 capillary column, respectively. All MS spectra were measured in the electron ionization (EI) mode. Cyclic voltammograms (CVs) were recorded using an Autolab PGSTAT 12, potentiostat/galvanostat at a scan rate of 100 mV $s^{-1}$ using a three-electrode cell, including Pt disk, Pt wire, and Ag/AgCl as the working electrode, the counter electrode, and the reference electrode, respectively. In all voltammetry experiments, $Fe(\eta^5\text{-}C_5H_5)$ (ferrocene) ($E_{1/2}$ = 640 mV vs. NHE related to redox couple $Fc/Fc^+$ [38]) and TBAH were used as an internal reference and a supporting electrolyte, respectively. Following each electrolysis, an aliquot was taken both for GC and GC–MS analyses. Since the excess phenylpyridinium does not affect the electrocatalytic dechlorination of $CH_2Cl_2$ by the Re catalyst, a non-stoichiometric ratio was used to prepare the catalyst solution during the cyclic voltammetry measurements. Hence, the current intensity of the CV peaks differs from that expected for $(2\text{-ppyH})_2[ReCl_6]$.

### 2.2 X-ray crystallography

Single-crystal X-ray diffraction data of $(2\text{-ppyH})_2[ReCl_6]$ were collected by a Bruker Apex II CCD area–detector

diffractometer with MoKα radiation ($\lambda = 0.71073$ Å) at 100(2) K. Cell refinement, data collection, data reduction, and absorption correction (using the multi-scan method) were processed with Bruker software packages [39]. The structure of $(2\text{-ppyH})_2[ReCl_6]$ was solved by direct methods using SHELXS-97 [40]. The non–hydrogen atoms (C, O, Re, Cl, and N) were refined anisotropically by the full-matrix least–squares method on $F^2$ using SHELXTL [41]. The H atoms of the pyridyl rings were placed in calculated positions. Relevant crystallographic data for $(2\text{-ppyH})_2[ReCl_6]$ are listed in Table 1.

### 2.3 Computational details

The molecular structures and bonding features of the intermediates involved in the electrocatalytic mechanisms were calculated without symmetry restrictions by employing DFT calculations as implemented in the GAUSSIAN09 suite of programs [42] with the M06-L functional [43]. The effective core potential (ECP), LANL2DZ, for the Re atom and the 6–31 + G(d) basis-set for the light atoms (C, H, N, and Cl) were selected. The frequency was also calculated to provide all transition states, stationary points, and Gibbs free energies at 298.15 K. The intrinsic reaction coordinate calculations (IRC) were performed for further verification of the transition state structures. The polarized continuum model (PCM) was selected for modeling the solvent (acetonitrile).

**Table 1** Details of structure refinement and selected crystallographic data for $(2\text{-ppyH})_2[ReCl_6]\cdot 2H_2O$ complex

| Crystallographic data for $(2\text{-ppyH})_2[ReCl_6]\cdot 2H_2O$ | |
|---|---|
| CCDC No | 2,018,375 |
| Empirical formula | $C_{22}H_{24}Cl_6N_2O_2Re$ |
| Formula weight | 747.33 |
| $T$ (K) | 100 (2) |
| $a$ (Å) | 7.4710 (3) |
| $b$ (Å) | 9.0776 (4) |
| $c$ (Å) | 10.5802 (4) |
| $\alpha$ (°) | 69.180 (2) |
| $\beta$ (°) | 72.224 (2) |
| $\gamma$ (°) | 79.974 (2) |
| Z | 1 |
| Crystal size ($mm^3$) | 0.60 × 0.40 × 0.2 |
| Index ranges | $-12 \le h \le 13$<br>$-15 \le k \le 15$<br>$-16 \le l \le 17$ |
| Independent reflections | 6825 |
| Independent reflections [$I > 2\sigma(I)$] | 6816 |
| Data/restraints/parameters | 6825/3/154 |
| Final $R$ indices [$I > 2\sigma(I)$] | $R_1 = 0.018$, $wR_2 = 0.046$ |

### 2.4 Synthesis of $(2\text{-ppyH})_2[ReCl_6]$ complex

A mixture of $Re_2Cl_{10}$ (726 mg, 1 mmol), $AgNO_3$ (339 mg, 2 mmol), and 2–phenylpyridine (0.28 mL, 2 mmol) was added to a mixture of acetonitrile/water (6:1, 35 mL) and refluxed for 18 h under nitrogen atmosphere. The color of the reaction mixture changed from black to pale yellow during the reflux period. After cooling the reaction, the solution was filtered to remove the white AgCl precipitate. A yellow residue was obtained after the filtration and evaporation of the solution. Column chromatography ($Al_2O_3$, grade III, WA, 25 × 1 cm) was used for purification of the crude product. Elution with a mixture of chloroform/hexane (1:1 v/v) gave a pale yellow band of the pure $(2\text{-ppyH})_2[ReCl_6]$ complex, which was separated and evaporated to dryness. The resulting pale yellow powder was dissolved in DMF and then recrystallized by ether diffusion into the solution at 5°C. High-quality crystals of the hydrated complex $(2\text{-ppyH})_2[ReCl_6]\cdot 2H_2O$ were obtained after *ca.* two weeks. Yield: 514 mg (69%). Elemental Anal. Calcd. for $C_{22}H_{24}Cl_6N_2O_2Re$: C, 35.39; H, 3.25; N, 3.78. Found: C, 35.45; H, 3.27; N, 3.75%. IR (KBr; $\nu_{max}/cm^{-1}$): N–H (3477 (b, m)); C=N (1604 (m)); C=C (1580 (m)).

## 3 Results and discussion

### 3.1 Synthesis route

The abundant majority of hexachlororhenate anions which involve the $Re^{IV}$ oxidation state ($[ReCl_6]^{2-}$) have been extensively investigated structurally and reported in more than ten crystallographic studies [44–47]. Hexachlororhenate anions with the rare oxidation states of $Re^{V}$ [48] and $Re^{VI}$ [49] are scarce. The synthesis of pyridinium-based hexachlororhenate(IV) complexes has been previously studied through the reaction of $[ReCl_6]^{2-}$ with pyridine-based derivatives in the presence of an inorganic acid (such as HCl). The crystal structures of $[ReCl_6]^{2-}$ anions with pyridinium counterions were reported by Kochel [50], Merozinski [44], and Julve [51].

In the current study, a new and facile strategy for the synthesis of the mononuclear phenylpyridinium hexachlororhenate(IV) complex salt without using any inorganic acid is presented. The following reaction is suggested for the formation of the $(2\text{–ppyH})_2[ReCl_6]$ complex (Scheme 1).

### 3.2 Crystal structure

The structures of the molecular entities of the $(2\text{–ppyH})_2[ReCl_6]\cdot 2H_2O$ complex are displayed in Fig. 1. The rhenium(IV) atom is located on an inversion center and

**Scheme 1** Synthesis route to obtain $(2\text{–ppyH})_2[ReCl_6]$ complex

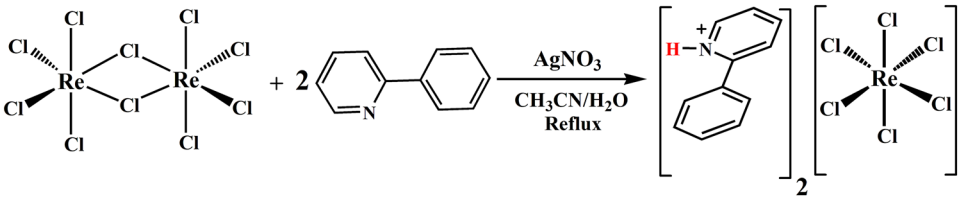


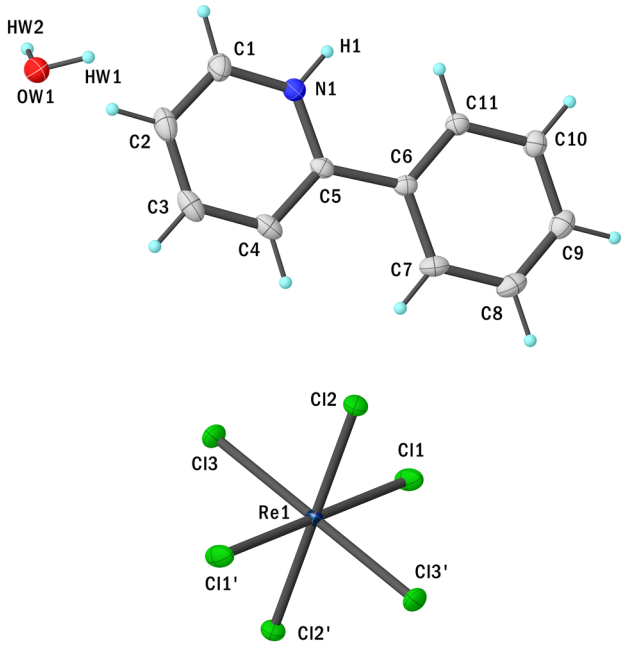


**Fig. 1** ORTEP view of the molecular entities in $(2\text{-ppyH})_2[ReCl_6]$ complex with atom-numbering scheme

shows a slightly distorted octahedral coordination environment with the six Re–Cl bonds lengths roughly equal to each other and the Cl–Re–Cl bond angles of approximately 90° (Table 2).

The aromatic rings in the $2\text{-ppyH}^+$ counterion are untwisted with respect to one another, with a dihedral angle of 1.51° between the phenyl and protonated pyridine ring, thus adopting the highest energy conformation [52]. Interestingly, the twist angle of the $2\text{-ppyH}^+$ counterion in our previous work on $(2\text{-ppyH})[ReO_4]$ was 40.49° [53], although, biphenyl compounds in the crystalline state prefer to be planar at room temperature [54]. In the crystal structure of $(2\text{-ppyH})_2[ReCl_6]$, N–H···O hydrogen bonds between the (2-ppyH) cation and the water molecule as well as O–H···Cl hydrogen bonds between the water molecule and the $[ReCl_6]^{2-}$ anion consolidate the crystal packing (Fig. 2).

Selected bond lengths (Å) and bond angles (°) for $(2\text{-ppyH})_2[ReCl_6]$ in the crystal (solid-state) and the optimized structure in the gas and solvent (acetonitrile) phases are listed in Table 2.

### 3.3 FT-IR and $^1$H NMR spectroscopies

The FT-IR spectra of $Re_2Cl_{10}$, 2-ppy, and $(2\text{-ppyH})_2[ReCl_6]$ complex are shown in Fig. 3. The band at 1586 $cm^{-1}$ is related to the C=N stretching vibration of neat 2-phenylpyridine, while the corresponding stretching mode for $(2\text{-ppyH})_2[ReCl_6]$ complex is red-shifted and observed at 1604 $cm^{-1}$. The bands at around 3300–3500 $cm^{-1}$ are attributed to the vibration of N–H and –OH bonds of amine and captured water in the crystal units, respectively. The bands around 1430–1560 $cm^{-1}$ are assigned to the stretching vibration of $2\text{-ppyH}^+$ rings.

$(2\text{-ppyH})_2[ReCl_6]$ was further analyzed using $^1$H NMR technique in DMSO–*d6* (Fig. 4, including labeling scheme for the protons). The $^1$H NMR spectrum shows nine protons for the aromatic region of $2\text{-ppyH}^+$ rings and one proton on the nitrogen atom ($N^+$–$H_1$) of the pyridinium ring. The doublet peak at 8.68 ppm is attributed to $H_2$. The $H_3$ protons are observed at 7.93 ppm. The peaks at 7.64 ppm are assigned to two $H_4$ protons. $H_5$ and $H_6$ are in the range of 7.3–7.4 ppm. The peak at 7.15 ppm is associated with $H_7$. The peak at 2.34 ppm moves down-field compared to the other protons due to the protonation of the nitrogen atom ($N^+$–$H_1$) of the pyridyl ring in $2\text{-ppyH}^+$. Despite the presence of paramagnetic anion $[ReCl_6]^{2-}$ in the solution, there is no paramagnetic broadening in the $^1$H NMR spectrum.

### 3.4 Electrocatalytic reaction

Before commencing the electrochemical remediation of $CH_2Cl_2$ catalyzed by $(2\text{-ppyH})_2[ReCl_6]$, we briefly discuss the cyclic voltammetric behavior of the pure catalyst to examine its electrochemical properties. The catalyst solution was prepared by dissolving 36 mg of $(2\text{-ppyH})_2[ReCl_6]$ (5.0 mM) in 10 mL of acetonitrile in the presence of 0.1 M TBAH under $N_2$ atmosphere. The cyclic voltammogram of the complex at a platinum disk electrode with a scan rate of 100 mV $s^{-1}$ is depicted in Fig. 5. The cyclic voltammogram of the complex in acetonitrile shows three couples centered at − 1.28, − 0.31, and + 1.17 V versus Ag/AgCl, which can be attributed to the Re(IV/III) couple [32, 55], $2\text{-ppyH}^+$ reduction [56, 57], and the Re(V/IV) reduction couple [32, 55], respectively. The essential feature of this voltammogram is the reduction couple at $E_{1/2} = -1.28$ V, including a single reduction wave in − 1.34 V and a single

**Table 2** Comparison of selected bond lengths (Å) and angles (°) for experimental data of the $(2\text{–ppyH})_2[ReCl_6]$ complex with the optimized structures from the DFT calculations

| Bond lengths (Å) and bond angles (°) | Crystal structure data | Computational structure data (MeCN) | Computational structure data (gas) |
|---|---|---|---|
| Re1–Cl1 | 2.3513 (3) | 2.3331 | 2.3378 |
| Re1–Cl1′ | 2.3513 (3) | 2.3331 | 2.3378 |
| Re1–Cl2 | 2.3674 (3) | 2.3755 | 2.3684 |
| Re1–Cl2′ | 2.3674 (3) | 2.3755 | 2.3684 |
| Re1–Cl3 | 2.3481 (3) | 2.3331 | 2.3378 |
| Re1–Cl3′ | 2.3481 (3) | 2.3331 | 2.3378 |
| Cl3—Re1—Cl1′ | 89.745 (13) | 90.0000 | 90.0000 |
| Cl3—Re1—Cl1 | 90.255 (13) | 90.0000 | 90.0000 |
| Cl1—Re1—Cl2 | 90.009 (13) | 90.0000 | 90.0000 |
| Cl1—Re1—Cl2′ | 89.991 (13) | 90.0000 | 90.0000 |
| Cl3—Re1—Cl3′ | 179.998 | 180.0000 | 180.0000 |

Symmetry-related atoms marked by a prime character are generated by symmetry code $-x+1, -y+2, -z$

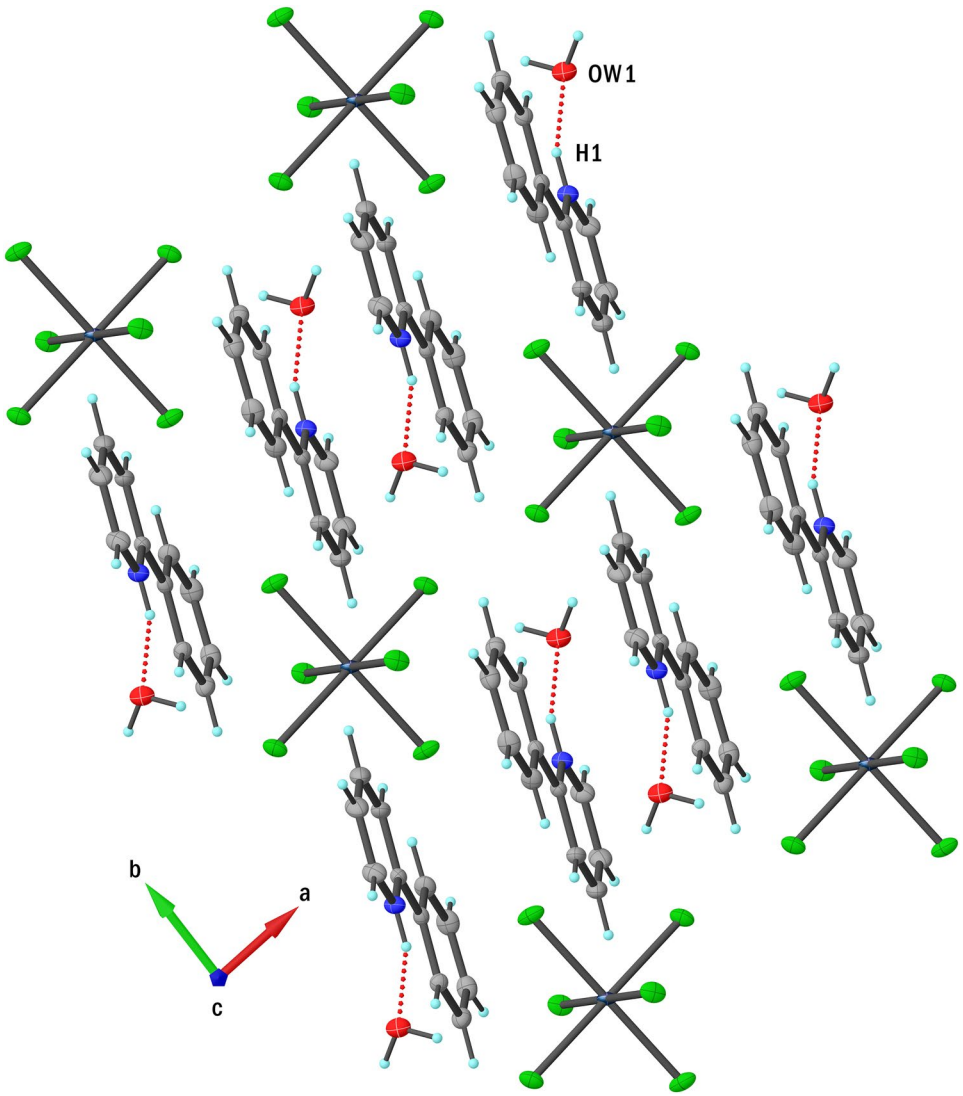


**Fig. 2** Crystal packing and intermolecular contacts of $(2\text{-ppyH})_2[ReCl_6]$ complex

oxidation wave located at − 1.22 V, which is related to the $[ReCl_6]^{3-/2-}$ redox couple. In addition, a reversible cyclic voltammogram for 2-phenylpyridinium is observed on the Pt electrode with anodic and cathodic waves at − 0.41 and − 0.21 V vs. Ag/AgCl, respectively (Fig. S2). Duyne et al. [57] investigated the electrochemical behavior of protonated heterocyclic amines, such as pyridinium salt. They discovered that the reduction of the pyridinium cation ($C_5H_5NH^+$) and its reversibility are unique features of the Pt working electrode. On the other hand, an irreversible cathodic peak was observed for the pyridinium solution at Ag, Au, and Cu electrodes [57].

Figure 6 shows the cyclic voltammograms for the dechlorination of $CH_2Cl_2$ at a platinum electrode in a 10 mL oxygen-free acetonitrile solution containing 5.0 mM of the complex. Curve A demonstrates a reversible voltammogram of the complex in a 0.1 M electrolyte solution. Curves B-E are the voltammograms recorded for the solutions containing the catalyst and various concentrations of $CH_2Cl_2$ (0.15, 0.6, 0.9, and 1.5 M, respectively). For curve B, a new cathodic peak is observed at − 1.76 V. According to previous studies [32], this new cathodic peak is followed by a one-electron reduction of $Re^{IV}$ to $Re^{III}$, assigned to the catalytic conversion of $CH_2Cl_2$ to a $CH_2Cl^{\bullet}$ radical by the electrogenerated $Re^{III}$ species. Notably, the anodic peak at − 1.22 V is decreased significantly from what is observed in curve A due to the interaction of the $Re^{III}$ chloride species with $CH_2Cl_2$. The cathodic peak is raised by increasing the concentration of $CH_2Cl_2$ from 0.15 to 0.6 M. Curve D in Fig. 6 displays the cyclic voltammogram for the solution of 0.9 M $CH_2Cl_2$ in the presence of the catalyst, which generates a larger cathodic peak at $E_{pc} = -1.76$ V. Interestingly, by increasing the concentration of $CH_2Cl_2$, the anodic peak at − 1.22 V vanishes, which is a result of the strong interaction between $CH_2Cl_2$ and the $Re^{III}$ species.

Ultimately, curve E displays the cyclic voltammogram for a solution containing 1.5 M $CH_2Cl_2$. A comparison of curves D and E reveals that the enhancement of $CH_2Cl_2$ in the complex solution (5 mM) is insignificant. Curve E is similar to curve D in which the anodic peak for the oxidation wave is no longer existent. As shown in Fig. 6, the increase in the $CH_2Cl_2$ concentration to 0.9 M leads to the creation of an oxidation wave at $E_{pa} = +1.39$ V. The observed peak is attributed to the production of the free chloride anion, evidenced by comparison with the cyclic voltammogram recorded for $[NBu_4]Cl$ in the complex-$CH_2Cl_2$ solution (Fig. S3). Equations 3–5 demonstrate the following chemical reactions for the formation of the species involved in the electrocatalytic reaction:

$$\left[ReCl_6\right]^{2-} + e^- \rightarrow \left[ReCl_6\right]^{3-} \quad (3)$$

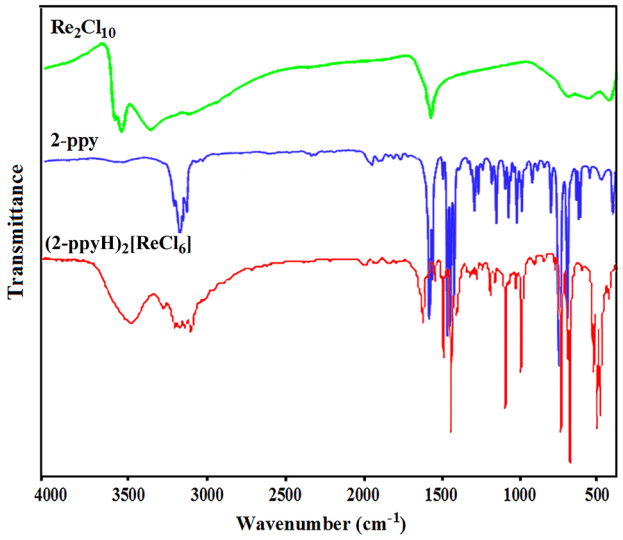


**Fig. 3** FT-IR spectra of $Re_2Cl_{10}$, 2-ppy, and $(2\text{-ppyH})_2[ReCl_6]$ complex

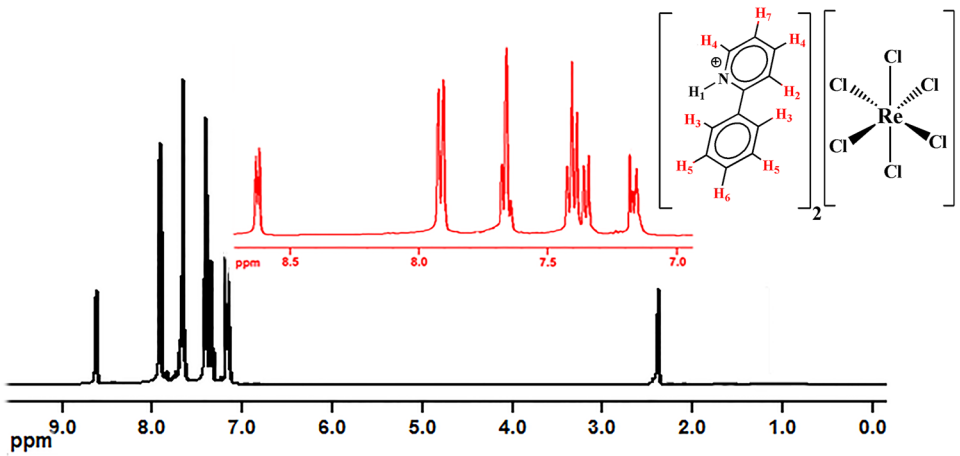


**Fig. 4** Room–temperature 400 MHz $^1H$ NMR spectrum of $(2\text{-ppyH})_2[ReCl_6]$ in DMSO–*d6*

$$\left[ReCl_6\right]^{3-} \rightarrow \left[ReCl_5\right]^{2-} + Cl^- \quad (4)$$

$$\left[ReCl_5\right]^{2-} + CH_2Cl_2 \rightarrow \left[ReCl_6\right]^{2-} + CH_2Cl^{\cdot} \quad (5)$$

Figure 7 shows a comparison of cyclic voltammograms containing 0.15 mM dichloromethane and various concentrations of the $(2\text{-ppyH})_2[ReCl_6]$ complex in an $N_2$ saturated TBAH/$CH_3CN$ solution at room temperature. The reduction peak raises as the $Re^{IV}$ complex concentration increases from 0.5 to 5 mM.

For evaluating the stability of the $Re^{IV}$ complex in the electrocatalytic reaction, the cycling stability of the catalyst was measured continuously at a scan rate of 100 mV $s^{-1}$ for 50 cycles. The catalyst exhibits high retention at current density after 50 CV cycles, indicating stability and reproducibility of the catalyst.

### 3.5 Controlled potential electrolysis of $Re^{IV}$-chloride in the presence of $CH_2Cl_2$

The bulk electrolysis of $CH_3CN$/TBAH solutions containing 5.0 mM of the hexachlororhenate(IV) complex was carried out at a platinum electrode held at a potential of − 1.34 V which was sufficient to generate the unsaturated $Re^{III}$-chloride in the presence of 1.5 M dichloromethane after various time intervals. Table 3 summarizes the electrolysis results corresponding to the electrocatalytic dechlorination of $CH_2Cl_2$ by the rhenium(IV) complex. The presence of 1,2-dichloroethane (EDC) was confirmed as the final product of the C–Cl bond cleavage process of $CH_2Cl_2$ by GC and GC–MS analyses. Figs. S4–10 depict typical GC and GC–MS analyses of the samples obtained from the electrolysis experiments using 5 mM solutions of the

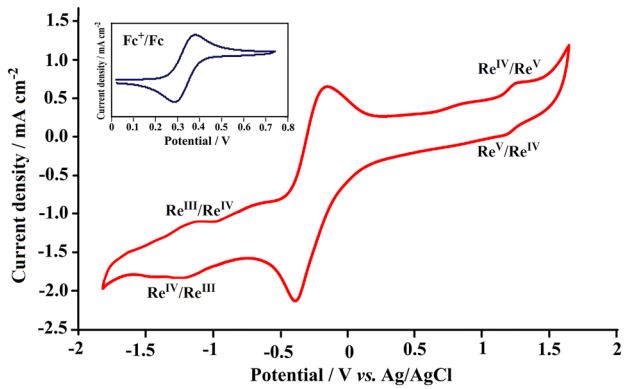


**Fig. 5** Cyclic voltammogram for $(2\text{-ppyH})_2[ReCl_6]$ complex (5.0 mM) in an oxygen-free acetonitrile solution with 0.1 M TBAH as the supporting electrolyte. The inset demonstrates the CV of ferrocene in an $N_2$ saturated electrolyte solution at a Pt electrode

$(2\text{-ppyH})_2[ReCl_6]$ complex in the presence of 1.5 M dichloromethane after various times. The electrolysis results demonstrate that the electrocatalytic mechanism is straightforward, and no side reactions are observed. As observed for entry 1 in Table 3, the catalyst shows the catalytic conversion of dichloromethane to 1,2-dichloroethane with a substantial yield of 23% at a reaction time of 30 min. After 60 min of the electrolysis, a 41% conversion rate was identified by GC analyses. Entries 3 and 4 in Table 3 are the results of two controlled potential electrolysis experiments of 1.5 M dichloromethane in the presence of $Re^{IV}$-chloride after 90 and 120 min, respectively. At − 1.34 V, the bulk electrolysis for entries 3 and 4 results in the conversion of dichloromethane to 1,2-dichloroethane in 64 and 88% yield, respectively. The turnover number (TON: no. moles of 1,2-dichloroethane formed per no. moles of $(2\text{-ppyH})_2[ReCl_6]$) achieved 132 after 2 h.

### 3.6 DFT evaluation of the proposed mechanism

A proposed electrocatalytic mechanism for the conversion of $CH_2Cl_2$ by the hexachlororhenate(IV) electrocatalyst is displayed in Scheme 2.

DFT calculations using the M06-L functional were employed to optimize the molecular structures of the species involved in the reaction mechanism in both gas and solvent (acetonitrile) phases. The optimized structures of the intermediates and transition state are depicted in Scheme 3 for the solvent phase ($CH_3CN$).

For each species in the pathway, the Gibbs free energies of the gas phase ($G^\circ_{gas}$) and solvation ($\Delta G^\circ_{solv}$) in acetonitrile were calculated and summarized in Table 4.

The calculated Gibbs free energy changes ($\Delta G^\circ_g$ and $\Delta G^\circ_{sol}$) of each step are listed in Table 5. The calculation method for determining the Gibbs free energies in both phases has been previously explained in the literature [58, 59]. In brief, the gas phase Gibbs free energy change ($\Delta G^\circ_g$) and the Gibbs free energy change in the solution ($\Delta G^\circ_{sol}$) are calculated using Eqs. (6) and (7).

$$\Delta G^\circ_{gas} = G^\circ_{gas}(B) - G^\circ_{gas}(A) \quad (6)$$

$$\Delta G^\circ_{sol} = \Delta G^\circ_{gas} + \Delta G_{sol}(B) - \Delta G_{sol}(A) \quad (7)$$

$G^\circ_{gas}(B)$ and $G^\circ_{gas}(A)$ are the standard gas-phase Gibbs free energy of the product (B) and reactant (*A*), respectively. $\Delta G_{sol}(B)$ and $\Delta G_{sol}(A)$ are the free energy of solvation of the products and reactant, respectively.

According to the proposed mechanism, the one-electron reduction (step I) of $[ReCl_6]^{2-}$ gives **Int.1**, which is predicted to be spontaneous by − 316.60 kJ $mol^{-1}$ in the solvent phase. The resulting **Int.1** shows an elongation

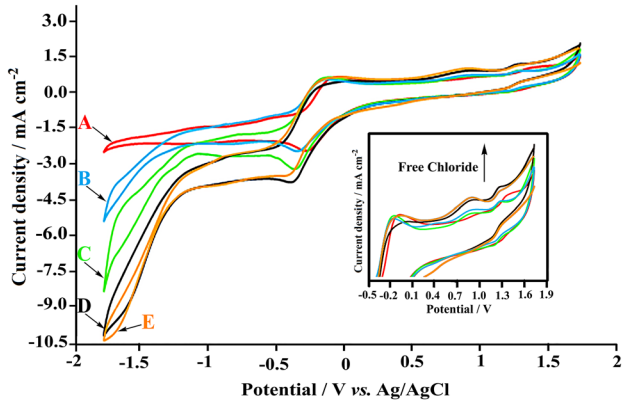


**Fig. 6** Cyclic voltammograms recorded in an $N_2$ saturated acetonitrile solution containing 0.1 M TBAH and 5.0 mM $(2\text{-ppyH})_2[ReCl_6]$ and the following concentrations of $CH_2Cl_2$: **a** 0 M, **b** 0.15 M, **c** 0.6 M, **d** 0.9 M, and **e** 1.5 M. The inset shows the oxidation waves at $E_{pa} = +1.39$ V assigned to the free chloride onion

of the Re–Cl bond from 2.412 Å in the primary catalyst to 2.495 Å. The $[ReCl_6]^{3-}$ species (**Int.1**) has a significant negative charge density, which leads to the dissociation of $Cl^-$ from the rhenium moiety. The cleavage of the Re–Cl bond in **Int.1** yields a chloride anion and a five-coordinated $Re^{III}$-chloride species with a square pyramidal configuration. This dissociation process (step II) is nonspontaneous by + 1.60 kJ $mol^{-1}$. The unsaturated five-coordinated rhenium(III) species (**Int.2**) can abstract the chlorine atom from $CH_2Cl_2$ through a transition state ($\mathbf{TS_{2\text{-}c}}$), in which the reduced **Int.2** is oxidized by $CH_2Cl_2$ to give an organic radical ($CH_2Cl^{\bullet}$) and the primary catalyst. The transition state for the transfer of the chlorine atom to the central Re atom is located with a calculated barrier energy

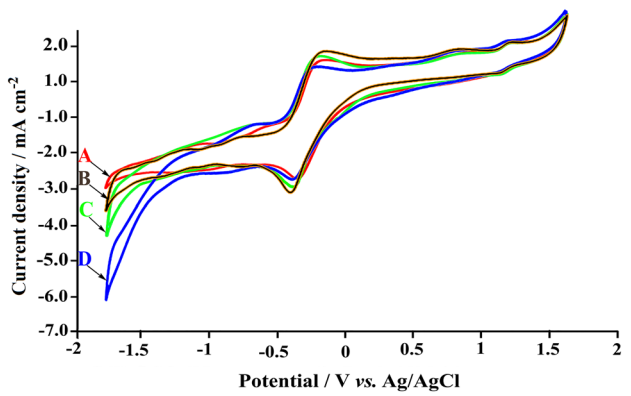


**Fig. 7** Cyclic voltammograms recorded in an $N_2$ saturated TBAH/$CH_3CN$ solution containing 0.15 mM $CH_2Cl_2$ and different concentrations of $(2\text{-ppyH})_2[ReCl_6]$ complex: **a** 0.5 mM, **b** 1.0 mM, **c** 2.0 mM, and **d** 5.0 mM

of + 16.53 kJ $mol^{-1}$ in the solvent phase. The energy profile for the transition state $\mathbf{TS_{2\text{-}c}}$ in acetonitrile is shown in Fig. 8. In the gas phase, the activation energy barrier of the transition state corresponding to the transfer of the chlorine atom is determined to be + 21.25 kJ $mol^{-1}$, which is higher than the corresponding value in the solvent phase (Fig. S11). The formation of $\mathbf{TS_{2\text{-}c}}$ is due to the addition of $CH_2Cl_2$ to the **Int.2** by a partially formed Cl···Re bond (2.671 Å), resulting in the elongation of the C···Cl bond from 1.78 to 1.88 Å. The abstraction of the chlorine atom from $CH_2Cl_2$ by the $Re^{III}$ species is spontaneous by − 37.95 kJ $mol^{-1}$. Furthermore, the DFT calculations reveal that the electrochemical pathway for the conversion of $CH_2Cl_2$ in the presence of $Re^{IV}$ complex salt is thermodynamically favorable in both gas and solvent phases ($\Delta G^{\circ}_{sol} = -68.16$ and − 352.96 kJ $mol^{-1}$ in the gas and solvent phases, respectively).

In addition, a detailed DFT study was carried out to evaluate the dechlorination of the second chlorine atom of dichloromethane in the presence of $[ReCl_6]^{2-}$. The proposed structures of the optimized key intermediates and transition state in the solvent phase are schematically depicted in Fig. 9. As the process progresses from **Int.2** to the initial catalyst, a new transition state ($\mathbf{TS'_{2\text{-}c}}$) can be introduced. For the transition state $\mathbf{TS'_{2\text{-}c}}$, the second chlorine atom is transferred from $CH_2Cl^{\bullet}$ to the rhenium moiety. The barrier energy for the second chlorine transfer is + 89.96 kJ $mol^{-1}$ in this pathway, which is greater than the barrier energy for the first chlorine in the same step (+ 16.53 kJ $mol^{-1}$).

The energy (eV) and distribution of the frontier molecular orbitals (FMOs) of the species involved in the mechanism are also represented in Fig. 10 for the solvent phase.

A frontier orbital analysis of the nucleophilic $CH_2Cl_2$ and electrophilic $ReCl_5^{2-}$ reactants (Scheme 4) demonstrates that the former's HOMO has a significant contribution at both chlorine and rhenium and the latter's HOMO has a $d\pi$ metal character.

## 4 Conclusion

We have studied a new and facile method for the synthesis of a mononuclear hexachlororhenate(IV) complex salt, $(2\text{-ppyH})_2[ReCl_6]$, and its application for the electrocatalytic remediation of dichloromethane. The $(2\text{-ppyH})_2[ReCl_6]$ complex salt was fully characterized by FT-IR, elemental analysis, $^1$H-NMR, and X-ray crystallography (as a dihydrate). The electrocatalytic system generates radicals from chlorinated organic compounds, which could serve in the dimerization reaction for the production of less chlorine-containing compounds. During the electrocatalytic reaction, the cathodic peak current of the dechlorination process raised by increasing the dichloromethane concentration. The

**Table 3** Electrocatalytic conversion of dichloromethane (1.5 M) to 1,2-dichloroethane by 5 mM $(2\text{-ppyH})_2[ReCl_6]$ complex electrogenerated at − 1.34 V in an $N_2$ saturated acetonitrile containing 0.1 M TBAH

| Entry | Time (min) | Temp. (°C) | Main product | Conv. (%) | TON |
|---|---|---|---|---|---|
| 1 | 30 | 25 | 1,2-dichloroethane | 23 | 34.5 |
| 2 | 60 | 25 | 1,2-dichloroethane | 41 | 61.5 |
| 3 | 90 | 25 | 1,2-dichloroethane | 64 | 96.0 |
| 4 | 120 | 25 | 1,2-dichloroethane | 88 | 132.0 |

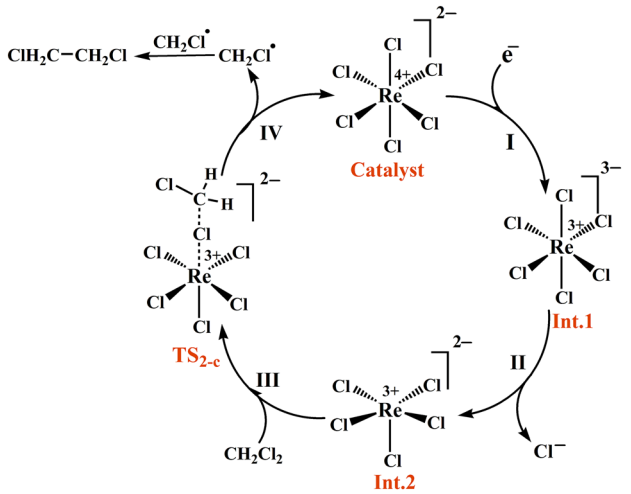


**Scheme 2** Proposed reaction mechanism for the electrocatalytic dechlorination of $CH_2Cl_2$ by the hexachlororhenate(IV) catalyst

electrocatalytic dechlorination process was further recorded at various concentrations of $(2\text{-ppyH})_2[ReCl_6]$. Furthermore, a mechanistic study of the electrochemical treatment of $CH_2Cl_2$ using hexachlororhenate(IV) as the catalyst was delineated. Density functional theory demonstrated that the proposed pathway is thermodynamically favorable in both gas and solvent phases. The DFT calculations were further applied to investigate the transition state ($\mathbf{TS_{2-c}}$) structure for the cleavage of the C–Cl bond in $CH_2Cl_2$ by a five-coordinated $Re^{III}$ moiety. The regeneration of the catalyst accompanied the transition state $\mathbf{TS_{2-c}}$ with the barrier energy values of + 16.53 and + 21.25 kJ $mol^{-1}$ in the gas and solvent phases, respectively. In addition, the DFT calculation was performed to evaluate the dechlorination reaction of the second Cl atom of $CH_2Cl_2$ in the presence of the Re catalyst. The transition state and activation energy for the second chlorine transfer were also calculated. As a consequence,

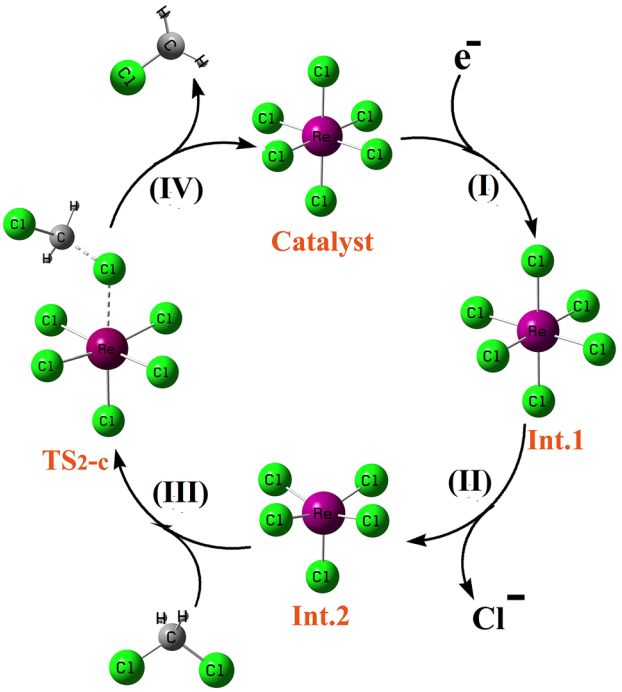


**Scheme 3** Optimized structures of the species involved in the reaction mechanism in the solvent phase ($CH_3CN$)

**Table 4** $G°_{(g)}$ (in Hartree) and $\Delta G°_{(solv)}$ (solvation in acetonitrile, kJ $mol^{-1}$) for the species involved in the proposed pathway

| Species | $G^o$(gas) | $\Delta G°$ (solvation) |
|---|---|---|
| Catalyst | − 2840.501919 | − 698.60 |
| Int.1 | − 2840.298135 | − 1550.26 |
| Int.2 | − 2380.243273 | − 715.05 |
| $CH_2Cl_2$ | − 959.646598 | − 10.49 |
| $CH_2Cl^•$ | − 499.410910 | − 4.56 |
| $Cl^-$ | − 460.261659 | − 290.66 |

**Table 5** $\Delta G°_g$ (gas phase, kJ $mol^{-1}$), and $\Delta G°_{sol}$ (solution phase, kJ $mol^{-1}$) of each step in the proposed pathway

| Step | $\Delta G°_g$ | $\Delta G°_{sol}$ |
|---|---|---|
| I | + 535.08 | − 316.60 |
| II | − 543.04 | + 1.60 |
| III + IV | − 60.25 | − 37.95 |

the activation barriers of this step in the gas phase and in $CH_3CN$ are + 21.50 and + 75.35 kJ $mol^{-1}$, respectively.

All kinds of research should be taken seriously to eliminate or reduce the pollution caused by chlorinated organic compounds, including insecticides and solvents.

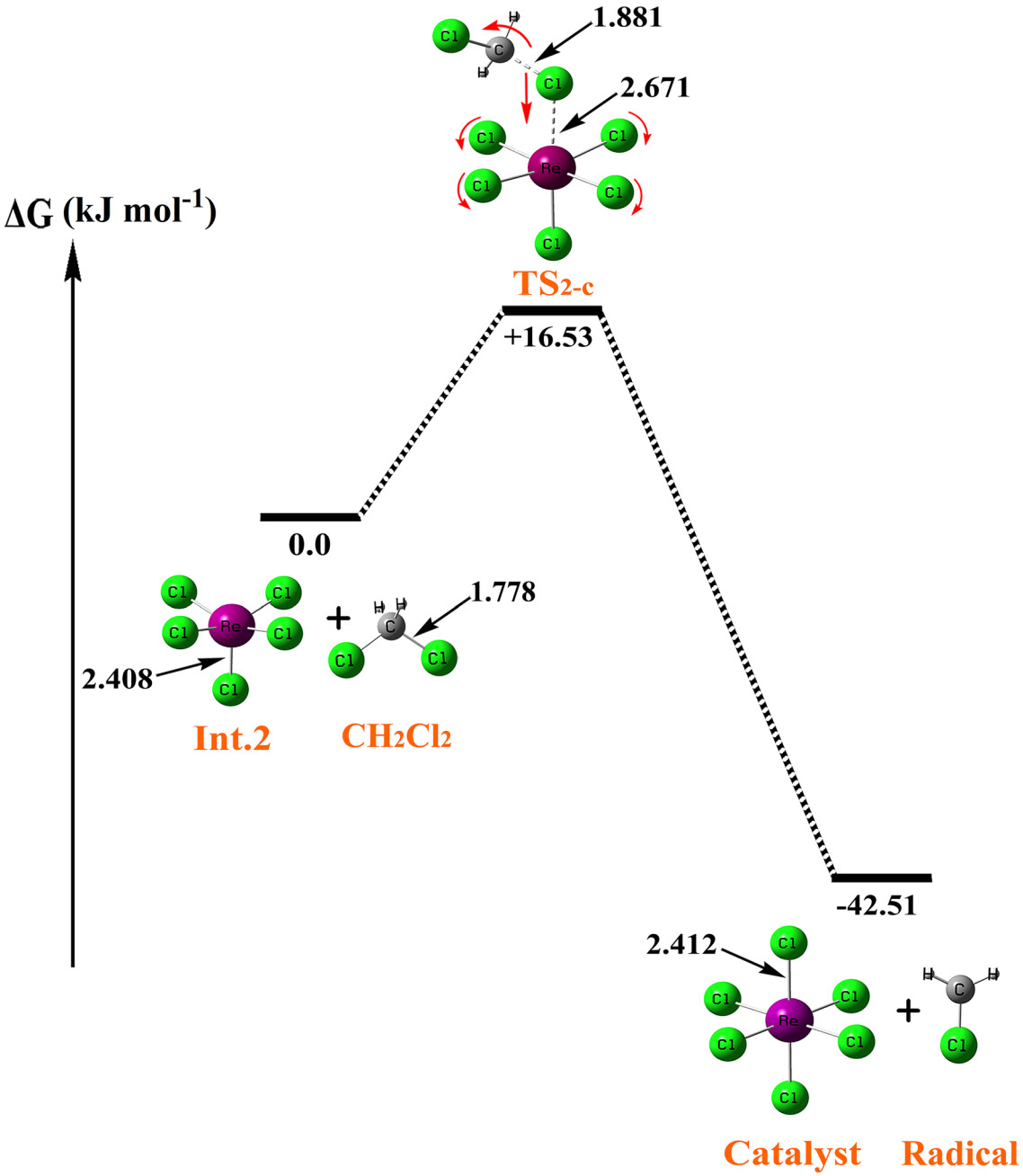


**Fig. 8** Calculated energy profile (kJ $mol^{-1}$, in acetonitrile) for the transfer of a chlorine atom from $CH_2Cl_2$ to the central Re atom of the complex. The red arrows show the displacements of the atoms of $\mathbf{TS_{2\text{-}c}}$ in the vibrational mode with imaginary frequency

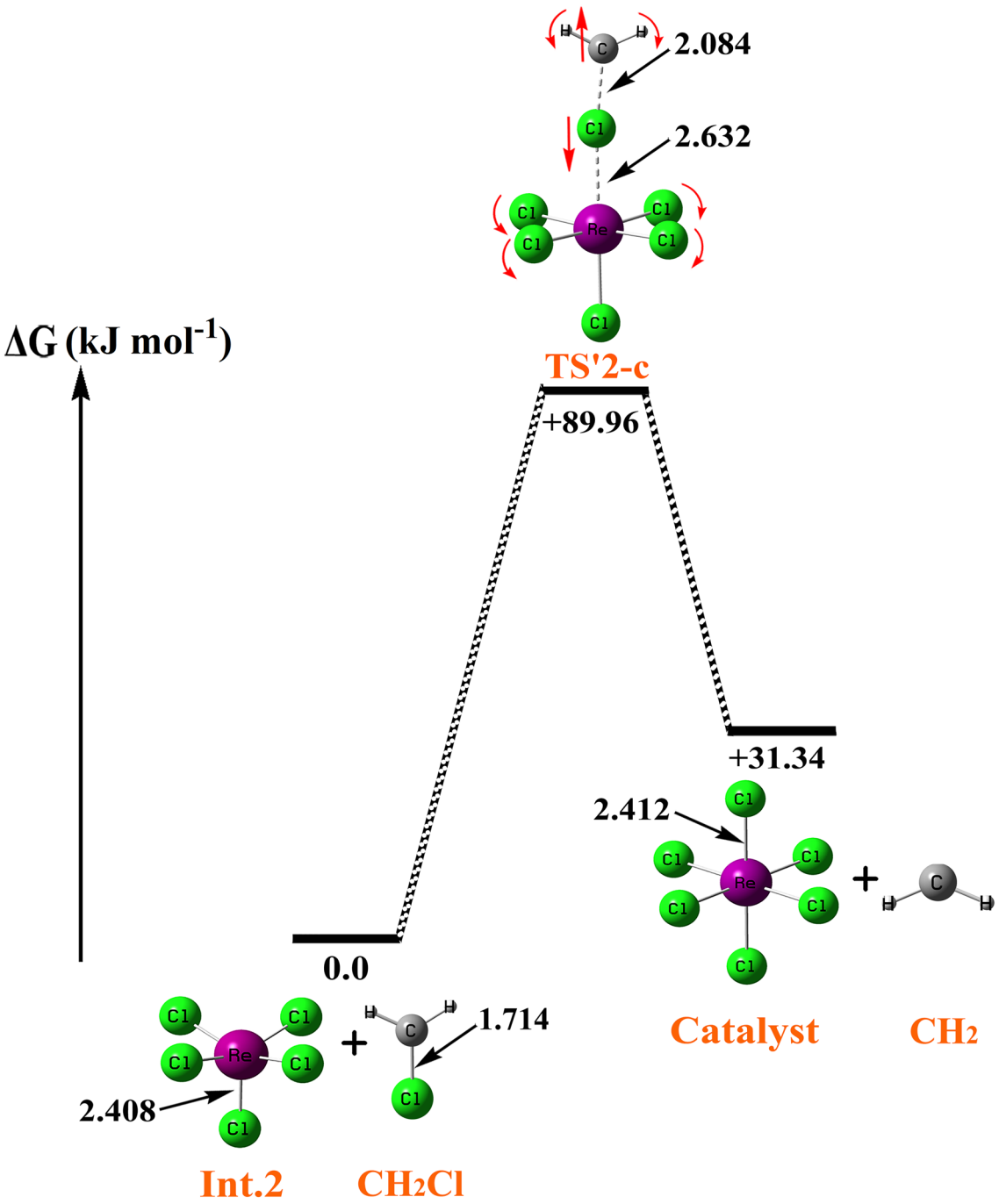


**Fig. 9** Calculated energy profile (kJ $mol^{-1}$, in acetonitrile) for the transfer of the second chlorine atom from $CH_2Cl^{\bullet}$ radical to the central Re atom of the complex. The red arrows show the displacements of the atoms of $\mathbf{TS'_{2\text{-}c}}$ in the vibrational mode with the imaginary frequency

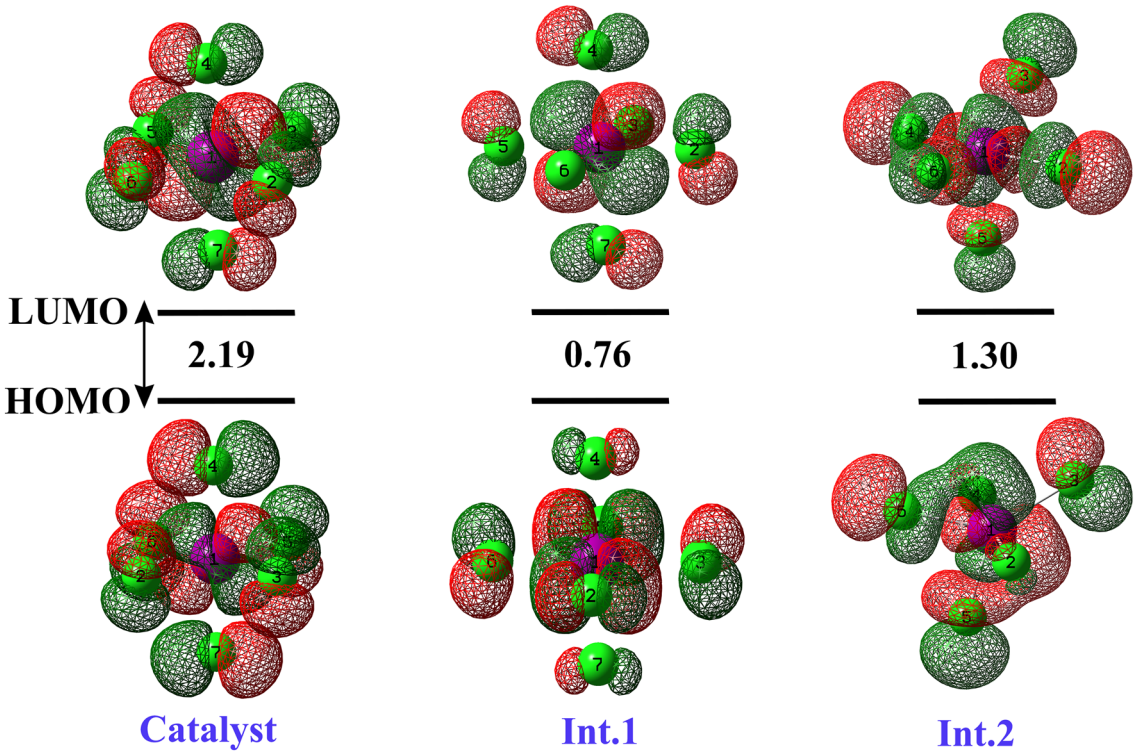


**Fig. 10** The energy (eV) and distribution of FMOs of the species involved in the mechanism in the solvent phase

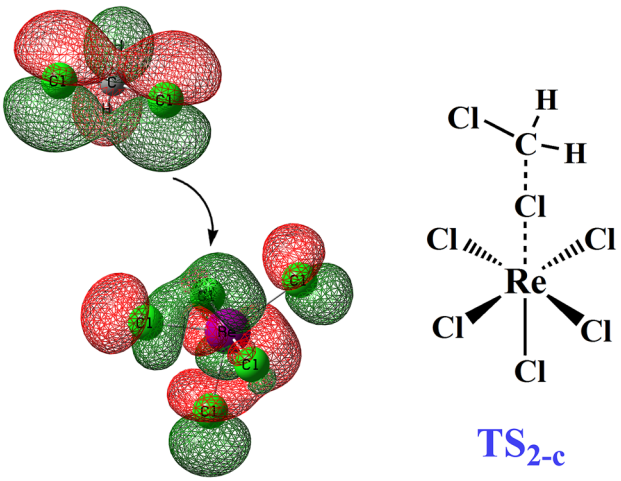


**Scheme 4** Frontier molecular orbitals of $CH_2Cl_2$ (HOMO) and $ReCl_5^{2-}$ (HOMO) in the solvent phase

**Supplementary Information** The online version contains supplementary material available at https://doi.org/10.1007/s10800-021-01607-4.

**Acknowledgements** We appreciate the Iran National Science Foundation (INSF) (Project No. 98011762). H. H. and M. W. are grateful to the X-ray center of TU Wien.

## References

1. Huang B, Lei C, Wei C, Zeng G (2014) Chlorinated volatile organic compounds (Cl-VOCs) in environment-sources, potential human health impacts, and current remediation technologies. Environ Int 71:118–138
2. Martin ET, McGuire CM, Mubarak MS, Peters DG (2016) Electroreductive remediation of halogenated environmental pollutants. Chem Rev 116(24):15198–15234
3. Zimmermann J, Halloran LJ, Hunkeler D (2020) Tracking chlorinated contaminants in the subsurface using compound-specific chlorine isotope analysis: a review of principles, current challenges and applications. Chemosphere 244:125476

4. Geneste F (2018) Catalytic electrochemical pre-treatment for the degradation of persistent organic pollutants. Curr Opin Electrochem 11:19–24
5. Aerts R, Van Overmeire I, Colles A, Andjelković M, Malarvannan G, Poma G, Den Hond E, Van de Mieroop E, Dewolf M-C, Charlet F (2019) Determinants of persistent organic pollutant (POP) concentrations in human breast milk of a cross-sectional sample of primiparous mothers in Belgium. Environ Int 131:104979
6. Xia D, Gao L, Zheng M, Sun Y, Qiao L, Huang H, Zhang H, Fu J, Wu Y, Li J (2019) Identification and evaluation of chlorinated nonane paraffins in the environment: a persistent organic pollutant candidate for the Stockholm Convention? J Hazard Mater 371:449–455
7. Li T, Li H, Li C (2020) A review and perspective of recent research in biological treatment applied in removal of chlorinated volatile organic compounds from waste air. Chemosphere 126338
8. McComb J, Mills I, Muller M, Berntsen HF, Zimmer KE, Ropstad E, Verhaegen S, Connolly L (2019) Human blood-based exposure levels of persistent organic pollutant (POP) mixtures antagonise androgen receptor transactivation and translocation. Environ Int 132:105083
9. Karak S, Dey K, Torris A, Halder A, Bera S, Kanheerampockil F, Banerjee R (2019) Inducing disorder in order: hierarchically porous covalent organic framework nanostructures for rapid removal of persistent organic pollutants. J Am Chem Soc 141(18):7572–7581
10. Hu Q, Liu S, Liu Y, Fang Xa XuJ, Chen X, Zhu F, Ouyang G (2019) Development of an on–site detection approach for rapid and highly sensitive determination of persistent organic pollutants in real aquatic environment. Anal Chim Acta 1050:88–94
11. Adhikary J, Meistelman M, Burg A, Shamir D, Meyerstein D, Albo Y (2017) Reductive dehalogenation of monobromo-and tribromoacetic acid by sodium borohydride catalyzed by gold nanoparticles entrapped in sol-gel matrices follows different pathways. Eur J Inorg Chem 11:1510–1515
12. Fiedler H, Kallenborn R, de Boer J, Sydnes LK (2019) The Stockholm convention: a tool for the global regulation of persistent organic pollutants. Chem Int 41(2):4–11
13. Srivastava V, Srivastava T, Kumar MS (2019) Fate of the persistent organic pollutant (POP) Hexachlorocyclohexane (HCH) and remediation challenges. Int Biodeterior Biodegrad 140:43–56
14. Šrédlová K, Škrob Z, Filipová A, Mašín P, Holecová J, Cajthaml T (2020) Biodegradation of PCBs in contaminated water using spent oyster mushroom substrate and a trickle-bed bioreactor. Water Res 170:115274
15. Chen Z, Liu Y, Wei W, Ni B-J (2019) Recent advances in electrocatalysts for halogenated organic pollutant degradation. Environ Sci Nano 6(8):2332–2366
16. Yinghua X, Yao Z, Mao Z, Shi M, Zhang X, Cheng F, Yang HB, bing Tao H, Liu B (2020) Single-ni-atom catalyzes aqueous phase electrochemical reductive dechlorination reaction. Appl Catal B Environ
17. Das SP, Ganguly R, Li Y, Soo HS (2016) Nucleophilic reactivity and electrocatalytic reduction of halogenated organic compounds by nickel o-phenylenedioxamidate complexes. Dalton Trans 45(34):13556–13564
18. Sonoyama N, Sakata T (2002) Conversion of CFC-13 to trifluoroacetic acid by electrochemical reaction with carbon dioxide. Chem Lett 31(4):444–445
19. Wagoner ER, Peters DG Electrocatalytic Reduction of 1, 1, 2-Trichloro-1, 2, 2-Trifluoroethane (CFC-113) at a Silver Cathode. In: Meeting Abstracts, 2012. The Electrochemical Society, vol 19, pp 2075–2075
20. Ming T, Caillol S, Liu W (2016) Fighting global warming by GHG removal: destroying CFCs and HCFCs in solar-wind power plant hybrids producing renewable energy with no-intermittency. Int J Greenhouse Gas Control 49:449–472
21. Sun Z, Shen H, Wei X, Hu X (2014) Electrocatalytic hydrogenolysis of chlorophenols in aqueous solution on $Pd_{58}Ni_{42}$ cathode modified with PPy and SDBS. Chem Eng J 241:433–442
22. Wagoner ER, Karty JA, Peters DG (2013) Catalytic reduction of 4, 4′-(2, 2, 2-trichloroethane-1, 1-diyl) bis (chlorobenzene)(DDT) with nickel (I) salen electrogenerated at vitreous carbon cathodes in dimethylformamide. J Electroanal Chem 706:55–63
23. Barnes JT, Adams RA, Hosseini S, Wagoner ER, Peters DG (2020) Nickel (I) salen-catalyzed reduction of 1, 1, 2-trichloro-1, 2, 2-trifluoroethane (CFC-113): $CO_2$-mediated carbon–fluorine bond cleavage. J Electroanal Chem 114002
24. Paramo U, Ibanez JG (2010) Catalytic behavior of cobalt (I) salen during the electrochemical reduction of lindane and hexachlorobenzene. J New Mater Electrochem Syst 13:356–360
25. Algarra AG, Braunstein P, Macgregor SA (2013) Computational study of the double C-Cl bond activation of dichloromethane and phosphine alkylation at $[CoCl(PR_3)_3]$. Dalton Trans 42(12):4208–4217
26. Li J, Li X, Wang L, Hu Q, Sun H (2014) C-Cl bond activation and catalytic hydrodechlorination of hexachlorobenzene by cobalt and nickel complexes with sodium formate as a reducing agent. Dalton Trans 43(18):6660–6666
27. McGuire CM, Hansen AM, Karty JA, Peters DG (2016) Catalytic reduction of 4, 4′-(2, 2, 2-trichloroethane-1, 1-diyl) bis (methoxybenzene)(methoxychlor) with nickel (I) salen electrogenerated at reticulated vitreous carbon cathodes. J Electroanal Chem 772:66–72
28. Wagoner ER, Hayes JL, Karty JA, Peters DG (2012) Direct and nickel (I) salen-catalyzed reduction of 1, 1, 2-trichloro-1, 2, 2-trifluoroethane (CFC-113) in dimethylformamide. J Electroanal Chem 676:6–12
29. Skljarevski S, Peverly AA, Peters DG (2011) Cyclic voltammetric and spectrophotometric investigation of the catalytic reduction of 1, 1, 2-trichloro-1, 2, 2-trifluoroethane (CFC-113) by electrogenerated cobalt (I) salen in dimethylformamide saturated with carbon dioxide. J Electroanal Chem 661(1):39–43
30. Gach PC, Karty JA, Peters DG (2008) Catalytic reduction of hexachlorobenzene and pentachlorobenzene by cobalt (I) salen electrogenerated at vitreous carbon cathodes in dimethylformamide. J Electroanal Chem 612(1):22–28
31. Fang Y, Al-Abed SR (2007) Palladium-facilitated electrolytic dechlorination of 2-chlorobiphenyl using a granular-graphite electrode. Chemosphere 66(2):226–233
32. Brown AR, Taylor KJ, Yellowlees LJ (1998) Catalytic carbon–chlorine bond cleavage via electrochemical reduction of $[ReCl_6]^{2-}$. J Chem Soc, Dalton Trans 14:2401–2404
33. Isse AA, Gennaro A, Lin CY, Hodgson JL, Coote ML, Guliashvili T (2011) Mechanism of carbon− halogen bond reductive cleavage in activated alkyl halide initiators relevant to living radical polymerization: theoretical and experimental study. J Am Chem Soc 133(16):6254–6264
34. Rosokha SV, Lukacs E, Ritzert JT, Wasilewski A (2016) Mechanism and thermodynamics of reductive cleavage of carbon-halogen bonds in the polybrominated aliphatic electrophiles. J Phys Chem A 120(10):1706–1715
35. Shandalov E, Zilbermann I, Maimon E, Nahmani Y, Cohen H, Adar E, Meyerstein D (2003) Mechanism of reduction of 2, 2-dibromomethyl-1, 3-propanediol by NiL-tetraazamacrocyclic complexes in aqueous solution− a pulse radiolysis and electrochemical study. Eur J Inorg Chem 22:4105–4109
36. Isse AA, Scarpa L, Durante C, Gennaro A (2015) Reductive cleavage of carbon–chlorine bonds at catalytic and non-catalytic

electrodes in 1-butyl-3-methylimidazolium tetrafluoroborate. Phys Chem Chem Phys 17(46):31228–31236
37. Lin CY, Coote ML, Gennaro A, Matyjaszewski K (2008) Ab initio evaluation of the thermodynamic and electrochemical properties of alkyl halides and radicals and their mechanistic implications for atom transfer radical polymerization. J Am Chem Soc 130(38):12762–12774
38. Cardona CM, Li W, Kaifer AE, Stockdale D, Bazan GC (2011) Electrochemical considerations for determining absolute frontier orbital energy levels of conjugated polymers for solar cell applications. Adv Mater 23(20):2367–2371
39. Bruker A (2012) saint and sadabs. Bruker Axs. Inc Madison, Wisconsin, USA
40. Sheldrick G (2008) SHELXTL, v. 2008/4. Bruker Analytical X-ray, Madison, WI
41. Sheldrick G (2016) SHELXL-2016/6: Program for Crystal Structure Determination. University of Göttingen, Göttingen, Germany
42. Frisch M, Trucks G, Schlegel H, Scuseria G, Robb M, Cheeseman J, Scalmani G, Barone V, Mennucci B, Petersson G (2009) Gaussian 09; Gaussian, Inc. Wallingford, CT 32:5648–5652
43. Zhao Y, Truhlar DG (2008) The M06 suite of density functionals for main group thermochemistry, thermochemical kinetics, noncovalent interactions, excited states, and transition elements: two new functionals and systematic testing of four M06-class functionals and 12 other functionals. Theoret Chem Acc 120(1–3):215–241
44. Mrozinski J, Kochel A, Lis T (2002) Crystal structure and magnetic properties of hexachlororhenates (IV) with aromatic amine cations. J Mol Struct 641(2–3):109–117
45. Bettinelli M, Di Sipio L, Valle G, Aschieri C, Ingletto G (1989) Crystal structures of three substituted ammonium hexachlororhenates (IV). Zeitschrift für Kristallographie-Crystalline Materials 188(1–4):155–160
46. González R, Romero F, Luneau D, Armentano D, De Munno G, Kremer C, Lloret F, Julve M, Faus J (2005) Hexachlororhenate (IV) salts of organic radical cations. Inorg Chim Acta 358(13):3995–4002
47. Piccinelli F, Bettinelli M, Cano J, Lloret F, Julve M, Dolmella A Magnetic properties of a new hexahalorhenate (IV) compound and structural comparison with its hexahaloplatinate (IV) analog. Eur J Inorgan Chem
48. Arp O, Preetz W (1994) Darstellung, Schwingungsspektren und Normalkoordinatenanalyse von Hexachlororhenat (V) sowie Kristallstruktur von $[P(C_6H_5)_4][ReCl_6]$. Z Anorg Allg Chem 620(8):1391–1396
49. Tamadon F, Seppelt K (2013) The elusive halides $VCl_5$, $MoCl_6$, and $ReCl_6$. Angew Chem Int Ed 52(2):767–769
50. Kochel A (2005) 2, 2′-Bipyrimidinium hexachlororhenate (IV) dihydrate. Acta Crystallogr Sect E: Struct Rep Online 61(4):m759–m760
51. Gryca I, Palion-Gazda J, Machura B, Penkala M, Kruszyński R, Cano J, Lloret F, Julve M (2015) Synthesis, crystal structure and magnetic properties of H 2 tppz $[ReCl_6]$ and [Cu $(bpzm)_2$ (μ-Cl) $ReCl_3$ (μ-ox) Cu $(bpzm)_2$ (μ-ox) $ReCl_3$ (μ-Cl)]n. Dalton Trans 44(39):17118–17128
52. Rickhaus M, Mayor M, Juríček M (2016) Strain-induced helical chirality in polyaromatic systems. Chem Soc Rev 45(6):1542–1556
53. Shakeri J, Hadadzadeh H, Farrokhpour H, Weil M (2019) A comparative study of the counterion effect on the perrhenate-catalyzed deoxydehydration reaction. Mol Catal 471:27–37
54. Grein F (2002) Twist angles and rotational energy barriers of biphenyl and substituted biphenyls. J Phys Chem A 106(15):3823–3827
55. Bennett MV, Long JR (2003) New cyanometalate building units: synthesis and characterization of [Re (CN)7]3 and $[Re(CN)8]_3$. J Am Chem Soc 125(9):2394–2395
56. Salaita G, Hubbard A (1992) Surface characterization of molecules at Pt (111) using leed, auger, hreels and electrochemistry in ultrahigh vacuum. Catal Today 12(4):465–479
57. Peroff AG, Weitz E, Van Duyne R (2016) Mechanistic studies of pyridinium electrochemistry: alternative chemical pathways in the presence of $CO_2$. Phys Chem Chem Phys 18(3):1578–1586
58. Shakeri J, Hadadzadeh H, Farrokhpour H, Joshaghani M, Weil M (2017) Perrhenate-catalyzed deoxydehydration of a vicinal diol: a comparative density functional theory study. J Phys Chem A 121(45):8688–8696
59. Shakeri J, Farrokhpour H, Hadadzadeh H, Joshaghani M (2015) Photoreduction of $CO_2$ to CO by a mononuclear Re (I) complex and DFT evaluation of the photocatalytic mechanism. RSC Adv 5(51):41125–41134